SHEAR-LAYER MANIPULATION OF BACKWARD-FACING STEP FLOW WITH FORCING: A NUMERICAL STUDY

Shia-Hui Peng

Swedish Defence Research Agency, FOI, Sweden

peng@foi.se

1 Introduction

By means of experimental and numerical analysis, turbulent flow separation has long been extensively studied. This is not only due to its interesting intrinsic flow features for fundamental studies, but also for its significance in engineering applications in relation to, among others, turbulent heat transfer, drag and noise generation. In the presence of sharp edges, protuberances, curvature surfaces and/or adverse pressure gradient, boundary layer separation is usually accompanied with free shear layer detaching from the wall surface and being characterized by consequent vortex motions and flow recirculation. Flow control of boundary layer separation has usually targeted to delay the separation onset in order to suppress the separation. In many cases, for example, to control the vortex motion behind a bluff body in relation to noise and drag generation, the modulation introduced by flow control actuators modifies the free shear layer stemmed from the separating point. By means of hybrid RANS-LS computations, the main purpose of the present work is to explore the manipulation on separated shear layer subjected to forcing-type actuation. A backward facing step (BFS) flow has thus been computationally analysed, with a focus on the free shear layer detaching from the step edge and reattached on the downstream bottom wall.

The separated shear layer of a BFS flow is often characterized by large-scale coherent vortical motions, corresponding to different types of instability, typically, a mixing-layer mode after detaching from the step and a low-frequency flapping mode for the interaction of the shear layer with the bottom wall (Chun and Sung, 1996). There have been many previous studies addressing the actuation on the BFS flows. Wu et al. (2013) measured the BFS flow with a rough step. It was shown that the reattachment length may significantly be affected by the roughness topography. Yoshioka et al. (2001a & b) investigated in their measurements turbulent flow features in the separated shear layer of a BFS flow actuated by periodic perturbations with a slit located at the step edge. The same experiment was reproduced in numerical computations using large eddy simulation by Dejoan and Leschziner (2004). Both have confirmed that a perturbation frequency at about St = 0.20, corresponding to the frequency of mixing-layer instabilities, may reduce the reattachment length by about 30%. In the experiment by Sujar-Garrido et al. (2013) and Benard et al. (2014), the BFS flow was manipulated with Dielectric Barrier Discharge (DBD) plasma actuators. With an expansion ratio of 10/9, the flow has a Reynolds number of Re = 30000, based on the bulk velocity, U_c = 15 m/s, and the step height, h = 30 mm. The DBD actuator was installed close the step edge, as shown in Figure 1. The surface discharge was produced by applying a high voltage sinusoidal signal on the exposed electrode. The experiment showed that the reattachment length was reduced from about $X_r = 6.0h$ for the baseline flow to about $4.6h$, provided that the DBD actuation is modulated with a frequency, f, corresponding to the frequency of the shear-layer mode, of which the measured value in terms of the Strouhal number ($St = fh/U_c$) is St = 0.25.

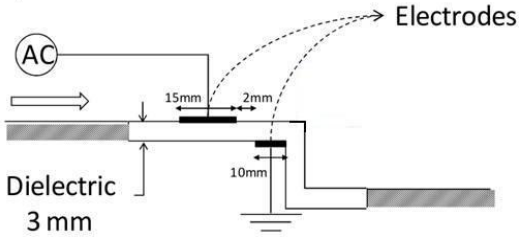

Figure 1: DBD actuator installed in the BFS flow measurement (Benard et al., 2014).

The BFS experiment with and without the DBD actuator by Benard et al. (2014) is taken here as a reference. It is emphasized that the purpose of the present work is to explore the adaptation of the separated shear layer to the manipulation of forcing-type actuation that has led to a reduced reattachment length similar to the measured value in the experiment using DBD plasma actuators. This has been achieved in the present simulations by incorporating forcing terms in the momentum equations.

2 Computational Setup and Methods

With the same BFS configuration as in the experiment by Benard et al. (2014), 2D RANS computations of precursor type were first conducted. The inflow section with freestream conditions has been set at about $x = -20h$ upstream of the step (located at $x = 0$), in order to approximately match the bounda-

ry layer velocity profile measured at the step edge. The downstream outflow section is placed at $x \approx 26h$. With symmetric boundary conditions, the top boundary is set at $y = 5h$ from the bottom wall. The 2D structured mesh has been particularly refined around the step, in the shear layer and in the recirculation region, as well as around the reattachment location and further downstream. The 3D mesh, consisting of about 7.6 million nodes and illustrated schematically in Figure 2, has been obtained by extending the 2D mesh over a spanwise extension of $2h$ with 80 uniform cells. Periodic boundary conditions are applied on the spanwise boundaries.

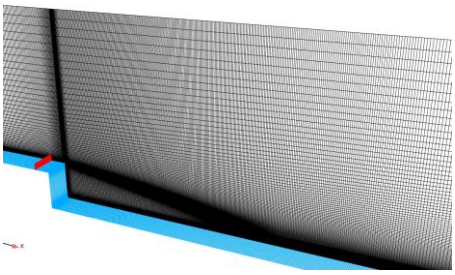

Figure 2: Computational grid. The red-coloured slice indicates the location where body forces are added.

The impact of DBD plasma actuator has often been modelled with a body force as a function of the electric field (E), the net charge density (ρ_c) and the forcing frequency (in relation to the duty cycle). Comprehensive work of modelling surface DBD-plasma actuation can be found in, e.g., Shyy et al. (2002) and Shang and Huang (2014). Instead of modelling the sophisticated details of DBD-plasma physics, in the present work, the unsteady impact of the DBD plasma actuator is integrated into forcing terms, f_x and f_y, which are then incorporated into the momentum equations in the streamwise and wall-normal directions, respectively (Suzen and Huang, 2006). The two components of the body force are cast respectively into an exponential function of wall distance in the form of $f_i = C_i \exp(-y/A_i)$ (Appelgren et al., 2009). Based on the experimental data (N. Benard, private communication), the body force is approximated to induce a steady-in-mean, two-dimensional ionized air flow with zero-pressure gradient. The imposed body force is aligned with the direction of the averaged body force derived from the measured ionized air speed. The forcing terms are imposed on a 2D plane with a height of 7.5 mm and located in the middle of the gap between the two DBD electrodes (x = -13 mm from the step edge, see Figures 1 and 2).

The impact of two types of forcing has been investigated. In the "*steady forcing*" the body forces, f_x and f_y, are continuously activated, of which the magnitudes have been scaled to assure that the shear layer is reattached downstream on the bottom wall at about the same location as measured for the controlled flow with the actual DBD actuator. In the experiment, Benard et al. (2014) has used unsteady forcing with a modulation frequency corresponding to the frequency of the shear-layer instabilities (at St = 0.25 as derived from experimental measurement). In our simulations, it has been noticed that the flapping motion of the separated shear layer is characterized by a frequency of St ≈ 0.08 with a rather large magnitude of power spectral density (PSD) at the step corner from which the shear layer is stemmed. In the present analysis, this "flapping" frequency has been adopted as the modulation frequency in conjunction with the same approximation of body forces used in the steady forcing. Hereafter, this modulated forcing is termed "*burst forcing*". The main purpose with the burst forcing has been to explore the impact of the excited flapping motion on the shear-layer flow properties. The results should be different from the measurement of Benard et al. (2014) with unsteady DBD forcing, where a different modulation frequency was used in harmonization with the shear-layer mode.

The computation has been conducted using the CFD code Edge (Eliasson, 2001), which is a node-based unstructured Navier-Stokes solver. The finite-volume scheme is second-order accurate in space for both the advection and diffusion. A dual-time stepping method is used for time marching, with the physical temporal discretization using a second-order backward approximation. Algebraic multigrid algorithm is employed in conjunction with an implicit residual smoothing scheme. The solver is parallelized using MPI. The time step used in all unsteady computations has been set to $\Delta t = 0.0667h/U_c$. In the statistical analysis, besides the time-averaging over a period of $750h/U_c$ or more, a spatial-averaging over the homogeneous spanwise direction has been further conducted.

3 Results and Discussion

The baseline flow has been computed using two hybrid RANS-LES models, the HYB0 model by Peng (2005) and the IDDES model by Shur et al. (2008). In Figure 3, a comparison is made for the time-averaged streamwise velocity, U, and the r.m.s of resolved streamwise velocity fluctuations, u_{rms}, obtained respectively with the HYB0 and IDDES models. For reference, the profiles of mean streamwise velocity computed with the S-A RANS model (Spalart and Allmaras, 1992) are also plotted. In general, the HYB0 and IDDES computations have given very similar predictions for the mean flow and resolved turbulent statistics. In the shear layer, the streamwise velocity has been somewhat under-predicted by the two hybrid RANS-LES models, and further downstream for $x/h > 2$ by also the RANS computation. The resolved turbulence at the step (not shown here) is rather small as expected in computations using conventional hybrid RANS-LES methods, due to the use of RANS mode in the near-wall layer. Such an under-prediction is further

reflected in the initial stage (at x/h =1) of the shear layer. Further downstream, the resolved turbulent fluctuation shows a relatively fast growth, as compared to the experimental data. Although not shown here, similar tendency has been observed in the predictions of other resolved turbulent quantities.

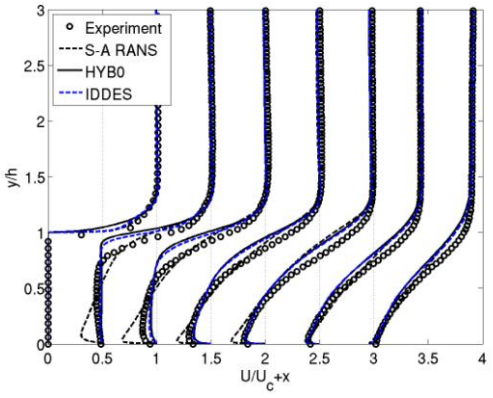

(a) Mean streamwise velocity, U.

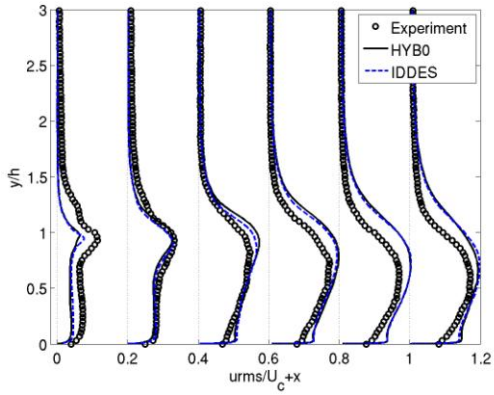

(b) Streamwise velocity fluctuations, u_{rms}.

Figure 3: Baseline BFS flow. Vertical profiles for U at x/h = 0, 1, 2, 3, 4, 5 and 6, and for u_{rms} at x/h = 1, 2, 3, 4, 5 and 6 (from right to left).

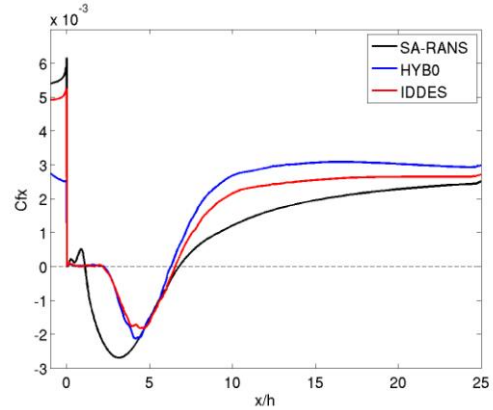

Figure 4: Baseline BFS flow. Distribution of skin friction coefficient, C_{fx}, on the bottom wall surface.

In comparison to X_r = (5.8–6.2)h, the HYB0, IDDES and S-A RANS models have produced a reattachment length of 6.17h, 6.34h and 6.45h, respectively. This is further highlighted in Figure 4 with the distributions of skin friction coefficient on the bottom wall surface. As also shown in Figure 3, the RANS computation predicts a relatively intensive reverse flow near the bottom wall in the recirculation region, as well as a more pronounced secondary bubble in the step corner as indicated by the skin friction in Figure 4.

With the same mesh as for the baseline flow, the HYB0 model has been used in the computations of the flow manipulated with steady forcing and burst forcing, respectively. The computation started with the HYB0-computed baseline flow by turning on the DBD forcing term for steady forcing, or by switching on/off the forcing term at a modulation frequency of St_m = 0.08 for burst forcing. It should be noted that the difference in the predictions presented below for the baseline flow and for the controlled flow has been caused by the incorporated "forcing" term, since the numerical settings have been kept the same in all these computations.

In the experiment it was found that the steady DBD actuation, established by means of a continuous AC high voltage signal with a magnitude of 24 KV and a frequency of f_{ac} = 1 KHz, has yielded only a 3% reduction of the reattachment length, X_r (Benard et al., 2014). Instead, a significant reduction of X_r was achieved by a burst-type actuation with a modulation frequency consistent to the measured frequency of shear-layer instabilities at St_{ms} = 0.25. In the numerical simulation with steady forcing, as mentioned above, the body-force vector has been approximated in terms of two forcing components projected respectively in the streamwise and wall-normal direction to achieve a reduction of X_r similar to the BFS flow manipulated with the experimental burst actuation. The impact of the experimental modulation frequency is thus not reflected in the simulation with steady forcing. Using the burst forcing in the simulation, the two streamwise and wall-normal forcing terms are the same as with the steady forcing, and the modulation frequency is set at St_{mf} = 0.08 to match the frequency of the shear-layer flapping motion.

In Figure 5, a snapshot of resolved turbulent structures is illustrated, respectively, for the baseline flow in Figure 5(a), for the controlled flow with steady forcing in Figure 5(b) and with burst forcing in Figure 5(c). It is shown that the shear layer after the step edge has been significantly modified by the steady or burst forcing in the controlled flow as compared to the baseline flow. More "rolling" structures of 2D type are formed after detaching from the step edge, which present earlier breakup into three-dimensional structures in the controlled flow. Progressing downstream and deflecting towards the bottom wall, paring process and hairpin-type structures are observed. In addition, as compared with the steady forcing, the burst forcing has induced a more intensive interaction between the shear layer and the recirculating flow beneath. The structures in the shear layer actuated with burst forcing are characterized by relatively larger length scales, possibly due to

the interaction with freestream flow and an increasing amalgamation of vortices due to a reinforced flapping motion excited by the forcing at a harmonized burst frequency.

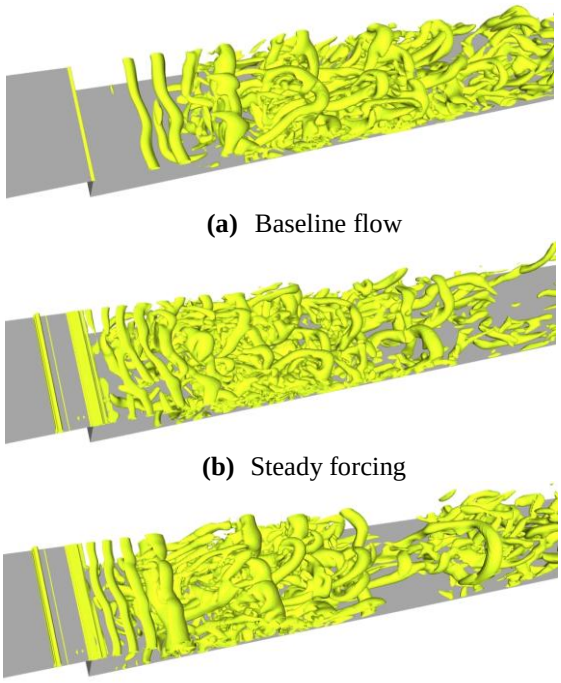

(a) Baseline flow

(b) Steady forcing

(c) Burst forcing

Figure 5: Snapshots of resolved turbulent structures in the form of iso-surface of *Q* criterion.

To reproduce the reduction of the reattachment length measured in the experiment, using steady forcing in the computation to represent the experimental DBD actuation, has led to a locally modified mean flow. This is shown in Figure 6, where the computed mean streamwise velocity profiles for the controlled flow (with steady and burst forcing) are compared to the measured data for the flow manipulated with the actual DBD plasma actuator. With the steady forcing activated on the DBD plane at x = -13 mm, both the RANS and HYB0 computations have induced local flow acceleration in the near-wall layer, which has further been reflected in the shear layer over the initial distance up to about $x/h \approx 3$. This has consequently increased the flow strain in close association to the formation of vortical structures in the initial stage of the shear layer. As for the baseline flow, the RANS computation has produced for the controlled flow a reverse flow in the recirculation bubble that is more intensive than those observed in the HYB0 computation and in the experimental measurement. Also shown in Figure 6 is the mean streamwise velocity for the flow manipulated with the burst forcing using the same forcing terms but being modulated with a frequency of St_{mf} = 0.08. In this case, the velocity profiles have accordingly responded to the further reduced recirculation bubble characterized by a relatively enhanced backflow. As shown, the local flow acceleration, induced by the steady forcing, in the incoming boundary layer and in the shear layer is absent in the computation when the forcing is modulated into burst type.

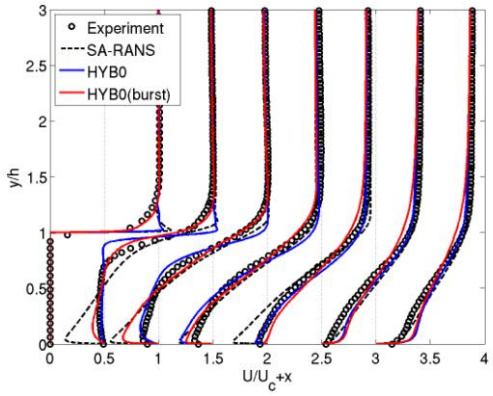

Figure 6: Time-averaged streamwise velocity for the baseline and controlled BFS flow at x/h = 0, 1 2, 3, 4, 5 and 6.

The skin friction along the bottom wall surface is illustrated in Figure 7, where the S-A RANS and HYB0 computations with steady forcing, as well as the HYB0 result due to burst forcing, are compared to the baseline flow predicted with the HYB0 model. The reattachment length is justified by C_{fx} = 0, at which the shear layer is reattached on the bottom wall and reversed in part toward the step corner. With steady forcing, the reattachment length is reduced to X_r = 4.80h being predicted by the S-A RANS model and to X_r = 4.59h for the HYB0 computation, as compared to the measured X_r = 4.60h using the actual DBD actuator with a modulation frequency of St_{ms} = 0.25. For the burst forcing with the modulation frequency St_{mf} = 0.08, the HYB0 computation has shown that the reattachment length is further reduced to X_r = 4.32h. It should be noted that a dramatic increase in C_{fx} is observed behind the location where the modelled DBD-induced forcing is introduced. This is an indication that both the steady and the burst forcing have accelerated the flow in the vicinity of the wall when approaching the step edge, from which the mixing layer is stemmed.

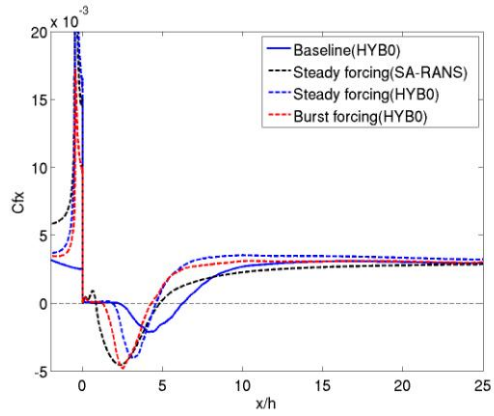

Figure 7: Distributions of skin friction coefficient, C_{fx}, on the bottom wall surface for the baseline flow and for the flow manipulated with forcing.

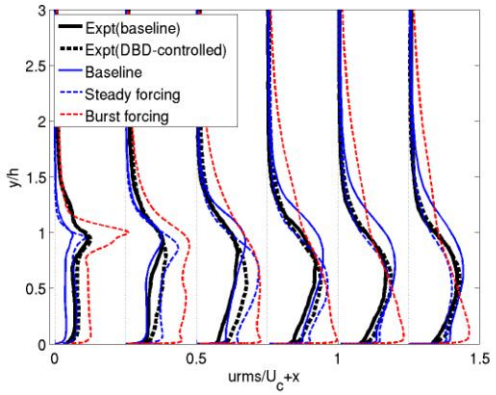

(a) Streamwise velocity fluctuations, u_{rms}.

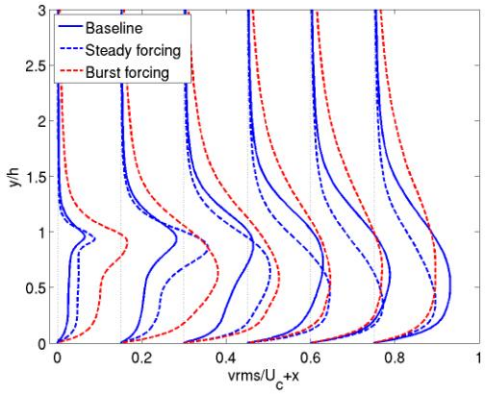

(b) Vertical velocity fluctuations, v_{rms}.

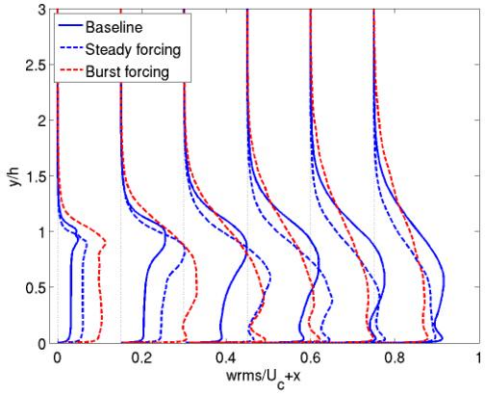

(c) Spanwise velocity fluctuations, w_{rms}.

Figure 8: Resolved turbulent fluctuations for the baseline flow and for the flow manipulated with forcing, at x/h = 1, 2, 3, 4, 5 and 6.

The resolved turbulent velocity fluctuations are plotted in Figure 8 at locations x/h = 1, 2, 3, 4, 5 and 6, respectively, in (a) for u_{rms}, in (b) for v_{rms} and in (c) for w_{rms}. It is noted that the experimental data for the controlled flow are not available for v_{rms} and w_{rms}. Manipulated with the modulated DBD actuation, the experiment shows that the streamwise velocity fluctuations in the controlled flow have been overall enhanced in the shear layer and in the recirculating flow. This tendency has been indicated by the computation with steady forcing for turbulent fluctuations in all directions. In the outer edge of the shear layer neighboring the freestream flow, on the other hand, the intensity of predicted velocity fluctuations with steady forcing becomes smaller than for the baseline flow. For the burst forcing modulated with St_{mf} = 0.08, the velocity fluctuations are overall intensified in the separated shear layer (note that $X_r = 4.32h$). This implies that turbulent diffusion has been enhanced in the shear layer, as compared to the baseline flow, as well as with the steady forcing that has targeted to reproduce the measured flow field manipulated by the actual DBD actuator with the modulation frequency St_{ms} = 0.25 in the experiment. Furthermore, for the burst forcing the resolved turbulent fluctuations becomes much extensive in the shear layer near the step (e.g., at x/h = 1) and in the recirculation bubble.

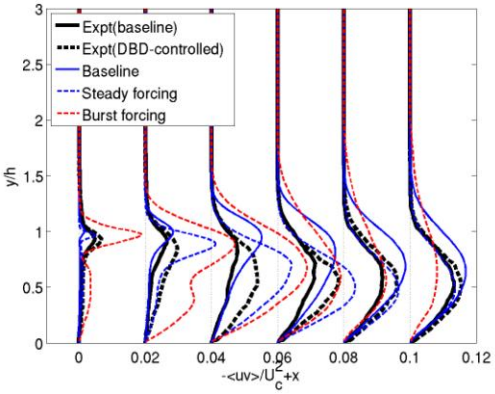

Figure 9: Resolved turbulent shear stress for the baseline flow and for the flow manipulated with forcing, at x/h = 1, 2, 3, 4, 5 and 6.

In Figure 9, the resolved turbulent shear stress, $-\langle uv \rangle$, is presented. For the baseline flow, the predicted turbulent stress is much larger than the measured data in the shear layer. The experimental measurement shows that the turbulent shear stress is overall enhanced in the shear layer and in the recirculation bubble, when the flow is manipulated with the DBD plasma actuator. With steady forcing and compared to the computed baseline flow, an increase in $-\langle uv \rangle$ has also been claimed, but not in the upper part of the shear layer, where $-\langle uv \rangle$ has been overpredicted for the baseline flow. The prediction for the controlled flow with steady forcing agrees better with the experiment after the reattachment (for the controlled flow at locations $x/h > 4$). Similar to the resolved turbulent velocity fluctuations shown in Figure 8, the computation with burst forcing has significantly enhanced $-\langle uv \rangle$ in the initial stage of the shear layer (up to x/h = 3) in comparison with the predictions for the baseline flow and for the controlled flow with steady forcing. This suggests that the burst actuation at St_{mf} = 0.08 has harmonized with the shear-layer flapping motion and enhanced the turbulence generation in the shear layer. This is further indicated by the thickness of the shear layer,

which becomes more extended in the upper part and presents a relatively rapid reduction of $-\langle uv \rangle$ downstream after the reattachment (at $X_r = 4.32h$).

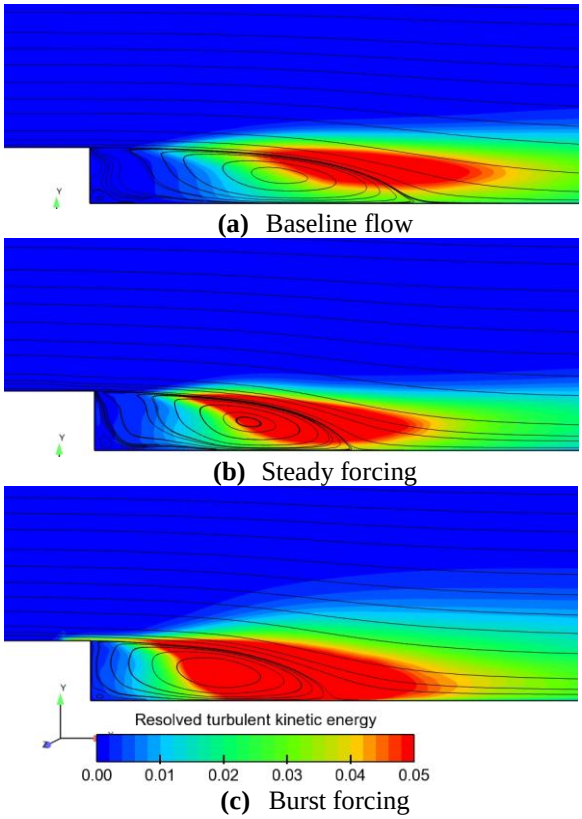

(a) Baseline flow

(b) Steady forcing

(c) Burst forcing

Figure 10: Contour of resolved turbulent kinetic energy for the baseline flow and for the controlled flow with steady forcing and burst forcing.

In comparison with the baseline flow, the role played by "forcing" in turbulence generation is further highlighted in Figure 10, where the contour of resolved turbulent kinetic energy (normalized with U_c^2) is illustrated. The mean flow streamlines are also plotted in the same figure. As expected, the most significant turbulence generation takes place in the separated shear layer. As already shown in Figure 3 for the baseline flow, the resolved turbulent fluctuations are under-predicted in the initial part of the shear layer, which has been commonly encountered in hybrid RANS-LES computations and being identified as the so-called "grey area". Nevertheless, it should be noted that the difference between the controlled flow in Figure 10(b) or (c) and the baseline flow in Figure 10(a) has been the outcome of manipulation using steady or burst forcing. For steady forcing, the region with significant turbulence generation is adapted to the earlier deflection of the shear layer for a reduced reattachment length, as compared to the baseline flow. As shown in Figure 10(a) and (b), both have pronounced a delayed establishment of a sensible level of turbulent kinetic energy after the shear layer is detached from the step. This may imply that the steady forcing has manipulated the separated shear layer, to a large extent, by means of momentum transfer. With the burst forcing, as shown in Figure 10(c), a relatively high level of turbulent kinetic energy has been induced in the wall layer on the top surface of the step and developed further downstream in the detached shear layer. Moreover, modulated with the frequency $St_{mf} = 0.08$, the burst forcing has triggered a more extended region of large turbulent energy, towards the bottom wall and above the separation bubble. In comparison with steady forcing, the predicted reattachment length is further reduced from $X_r = 4.59h$ to $4.32h$ by modulating the forcing. Obviously, the manipulation on the shear layer by the burst forcing is closely associated to turbulent energy generation and transfer process.

The manipulation on the shear layer by the forcing is further highlight by the power spectral density, PSD, of turbulent fluctuations. Figure 11 shows the PSD for the pressure fluctuations on the step edge, at $x/h = 0$ and $y/h = 1.0$. This is a location where the pressure fluctuation may sensibly respond to the formation of the rolling structures in relation to the initial shear-layer instabilities, the shear-layer flapping motion, as well as the associated oscillations of both the large recirculation and the secondary separation bubbles. For the baseline flow, the first two most distinguishable peaks, A and C in Figure 11, present at $St_A \approx 0.078$ and $St_C \approx 0.236$, respectively, and another less pronounced peak, B, located at $St_B \approx 0.158$. In the literature, see e.g., Yoshioka et al. (2001a), an optimal frequency has often been chosen in the range of the Strouhal number St = 0.18–0.27 for the manipulation of BFS flow, which matches the frequency of shear-layer instabilities of Kevin-Helmholtz type. This frequency was identified in the measurement by Benard et al. (2014) with a value of $St \approx 0.25$, which is close to $St_C \approx 0.236$ obtained in the present computation. The flapping motion of the shear layer indicates the interaction of the shear layer with the wall, which is characterized by a frequency of $St \approx 0.08$ (Sigurdson, 1995; Dejoan and Leschziner, 2004). This corresponds well to the low-frequency peak at $St_A \approx 0.078$ in the present computation for the baseline and controlled flows. The steady forcing does not modulate the shear-layer mode and the flapping motion, but has enhanced the fluctuations at high frequencies. Modulating the forcing with the frequency of flapping motion at St = 0.08, as shown in Figure 11, the burst forcing is harmonized with the flapping motion and has overall intensified the pressure fluctuation on the step edge, compared to the steady forcing. Moreover, it is noted that the burst forcing has induced a series of modes that present approximately a harmonic feature at frequencies of nSt_A ($n \geq 2$). The presence of harmonics might be due to nonlinear interaction between the mode of frequency St_A and the harmonic modes of frequency nSt_A (e.g., at St_B or St_C). The burst forcing at frequency St_A has reinforced the growth of other harmonics at higher frequencies. The growth of harmonics supports the merger of vortices in relation to the pairing process.

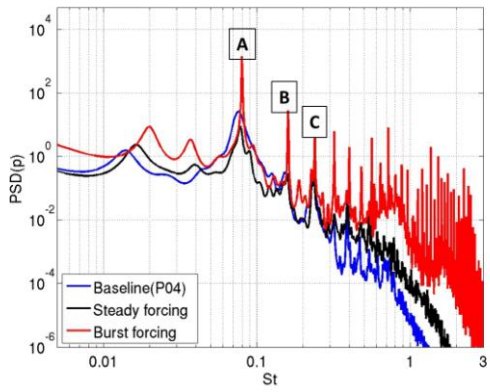

Figure 11: PSD of pressure fluctuations at the step edge (x/h = 0 and y/h =1.0).

In the shear layer, as shown in Figure 12, for the PSD of the pressure and vertical velocity fluctuations at x/h = 2 and y/h =1.0, the energy peaks of characteristic modes, corresponding to periodic flow phenomena or periodic passage of vortical structures, become less manifested in the baseline flow and in the flow manipulated with steady forcing. This suggests that, moving downstream, the periodic phenomena inherent in the shear layer have undergone increasing amalgamation in relation to the breakup of rolling structures and vortex pairing. With the burst forcing, most of the harmonics at high frequencies are absent in the shear layer, but those at frequencies St ≤ 0.48.

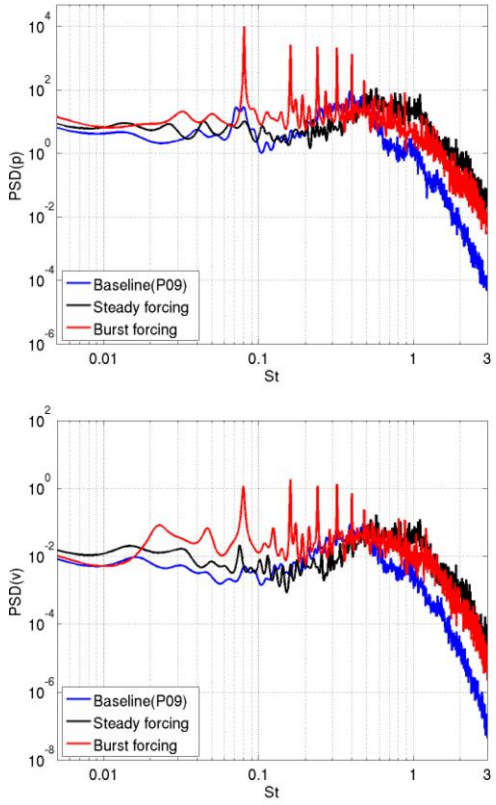

Figure 12: PSD of pressure fluctuations (upper) and vertical velocity fluctuations (lower) in the shear layer at x/h = 2 and y/h =1.0.

4 Summary and Conclusions

By means of hybrid RANS-LES computations, a numerical investigation has been undertaken for a backward-facing step flow manipulated with steady and burst forcing. The flow configuration is referred to the experimental measurement by Benard et al. (2014), where a DBD plasma actuator was used to manipulate the flow for a reduced reattachment length. The computation for the baseline flow has produced reasonable predictions for the mean flow in comparison with the experiment, although the turbulent stresses have been somewhat over-predicted in the downstream of the separated shear layer. The baseline flow computation has manifested a shear-layer flapping motion at the frequency St ≈ 0.078 and the shear-layer mode at St ≈ 0.236.

In the computation of the controlled flow, the impact of the DBD actuator has been modelled in terms of body forces being incorporated into the momentum equations as forcing terms. With steady forcing, the predicted reattachment length is reduced to 4.59h from 6.17h for the baseline flow, which is in good agreement with the experiment measurement. By modulating the forcing with a frequency of St_{mf} = 0.08 corresponding to the flapping motion of the shear layer, the burst forcing has manifested a further reduction of the reattachment length down to 4.32h in comparison to 4.60h forced by the experimental DBD actuation modulated with a frequency of the shear-layer mode at St_{ms} = 0.25.

In spite of some discrepancies in comparison to the available measured data for turbulent stresses, the computation with steady forcing has reasonably reflected the general tendency of changes of turbulent flow properties in the shear layer, similar to the experimental measurement. The steady forcing manipulates the shear layer by accelerating the near-wall flow and, consequently, introducing a steep velocity gradient to actuate the formation of initial shear-layer structures. With steady forcing, the most sensible enhancement of turbulence level takes place in the recirculation bubble. The burst forcing, on the other hand, triggers sensible turbulence generation in the wall layer detaching from the step, and has induced significant generation of turbulent energy in the shear layer and in the recirculation bubble. It may be confirmed that the effectiveness of steady forcing in manipulating the shear layer relies on the momentum transfer from the actuator to the detaching boundary layer, and the burst forcing may, additionally, actuate the process of turbulence generation and diffusion.

Compared to the baseline flow, both steady forcing and burst forcing have supported an earlier formation of 2D-type rolling structures and an earlier breakup of these structures. The burst forcing, with the frequency corresponding to shear-layer flapping motion, has pronounced a much diffusive shear layer with increased thickness. The modulation of the burst forcing has seemingly supported a series of harmonic modes, which may reinforce the interaction of vortices in the shear layer in relation to the paring process.

Nonetheless, the use of the modulation frequency in harmonization with the flapping motion need to be further examined.

Acknowledgements

The investigation conducted in this work was partially supported by the European research project MARS (2010-2014).

References

Appelgren, P., Hurtig, T., Skoglund, M. and Wallin, S. (2009), Electro-hydrodynamic flow control. FOI Report, FOI-R-2799-SE, Swedish Defence Research Agency, FOI, Stockholm.

Benard, N, Sujar-Garrido, P., Bayoda, K. D., Bonnet, J.P. and Moreau, E. (2014), Pulsed dielectric barrier discharge for manipulation of turbulent flow downstream a backward-facing-step. AIAA Paper 2014-1127.

Chun, K.B., Sung, H.J. (1996), Control of turbulent separated flow over a backward-facing step by local forcing. *Experiments in Fluids*, Vol. 21, pp.417–426.

Dejoan, A. and Leschziner, M. A. (2004), Large eddy simulation of periodically perturbed separated flow over a backward-facing step. *Int. J. Heat and Fluid Flow*, Vol. 25, pp.581-592.

Eliasson, P. (2001), EDGE: A Navier-Stokes solver for unstructured grids, Scientific Report, FOI-R-0298-SE, Swedish Defence Research Agency, Stockholm.

Peng, S.-H. (2005), Hybrid RANS-LES modelling based on zero- and one-equation models for turbulent flow simulation. In Proceedings of TSFP-4, Vol. 3, pp. 1159–1164.

Shang, J.S. and Huang, P.G. (2014), Surface plasma actuators modelling for flow control. *Progress in Aerospace Science*, Vol. 67, pp.29-50.

Shur, M., Spalart, P., Strelets, M., Travin, A. (2008), A hybrid RANS-LES approach with delayed-DES and wall-modelled LES capabilities. *Int. J. Heat and Fluid Flow*, Vol. **29**, pp.1638–1649.

Shyy, W., Jayaraman, B. and Andersson, A. (2002), Modelling of glow discharge-induced fluid dynamics. *J. App. Phys*., Vol. 92, pp.6434-6443.

Sigurdson, L.W. (1995), The structure and control of a turbulent reattaching flow. *J. Fluid Mechanics*, Vol. 298, pp.139-163.

Spalart, P.R. and Allmaras, S.R., (1992), A one-equation turbulence model for aerodynamic flows. AIAA Paper 92-0439.

Sujar-Garrido, P., Benard, N., Moreau, E. and Bonnet, J.P. (2013), Modifications of the shear layer downstream a backward facing step by dielectric barrier discharge plasma actuators. In Proc. TSFP-8.

Suzen, Y.B. and Huang, P. G. (2006), Simulation of flow separation control using plasma actuators. AIAA Paper 2006-877.

Wu, Y., Ren, H. and Tag, H. (2013), Turbulent flow over a rough backward-facing step. *Int. J. Heat and Fluid Flow*, Vol. 44, pp.155-169.

Yoshioka, S., Obi, S. and Masuda, S. (2001a), Organized vortex motion in periodically perturbed turbulent separated flow over a backward-facing step. *Int. J. of Heat and Fluid Flow*, Vol. 22, pp.301-307.

Yoshioka, S., Obi, S. and Masuda, S. (2001b), Turbulent statistics of periodically perturbed turbulent separated flow over a backward-facing step. *Int. J. of Heat and Fluid Flow*, Vol. 22, pp.393-401.